FEMS Yeast Research, 2023, 23, 1–10
DOI: 10.1093/femsyr/foad045
Advance access publication date: 18 October 2023
Research Article

Metabolic reconstruction of the human pathogen *Candida auris*: using a cross-species approach for drug target prediction

Romeu Viana[1,2], Tiago Carreiro[1,2], Diogo Couceiro[1,2], Oscar Dias[3], Isabel Rocha[4], Miguel Cacho Teixeira[1,2,*]

[1]Department of Bioengineering, Instituto Superior Técnico, University of Lisbon, 1049-001 Lisboa, Portugal
[2]iBB - Institute for Bioengineering and Biosciences, Associate Laboratory Institute for Health and Bioeconomy - i4HB, 1049-001 Lisboa, Portugal
[3]CEB - Centre of Biological Engineering, Universidade do Minho, 4710-057 Braga, Portugal
[4]ITQB Nova - Instituto de Tecnologia Química e Biológica António Xavier, 2780-157 Oeiras, Portugal
*Corresponding author. Department of Bioengineering, Instituto Superior Técnico, University of Lisbon, Av. Rovisco Pais 1049-001 Lisboa, Portugal. E-mail: mnpct@tecnico.ulisboa.pt
Editor: [Carol Munro]

Abstract

Candida auris is an emerging human pathogen, associated with antifungal drug resistance and hospital candidiasis outbreaks. In this work, we present iRV973, the first reconstructed Genome-scale metabolic model (GSMM) for *C. auris*. The model was manually curated and experimentally validated, being able to accurately predict the specific growth rate of *C. auris* and the utilization of several sole carbon and nitrogen sources. The model was compared to GSMMs available for other pathogenic *Candida* species and exploited as a platform for cross-species comparison, aiming the analysis of their metabolic features and the identification of potential new antifungal targets common to the most prevalent pathogenic *Candida* species. From a metabolic point of view, we were able to identify unique enzymes in *C. auris* in comparison with other *Candida* species, which may represent unique metabolic features. Additionally, 50 enzymes were identified as potential drug targets, given their essentiality in conditions mimicking human serum, common to all four different *Candida* models analysed. These enzymes represent interesting drug targets for antifungal therapy, including some known targets of antifungal agents used in clinical practice, but also new potential drug targets without any human homolog or drug association in *Candida* species.

Keywords: *C. auris*; Global stoichiometric model; gene essentiality; drug target; metabolic features

Research Highlights:

- Presenting the first genome scale metabolic model for the human pathogen *Candida auris*
- GSMM-based cross-Candida species comparison in search of unique metabolic features
- GSMM-based identification of a list of promising new drug targets

Introduction

Candida auris is an emerging human pathogen. First isolated in 2009 (Satoh et al. 2009), *C. auris* is geographically non-restricted (Ademe and Girma 2020) and thrives in nosocomial environments (M. N. Kim et al. 2009). While *Candida albicans* is still the most frequent etiological agent of candidiasis, a shift towards non-*Candida albicans Candida* species (NCAC) (Lass-Flörl 2009) has been registered since the 1990 s (Lass-Flörl 2009). Among the NCAC, *Candida glabrata*, *Candida parapsilosis* and *Candida tropicalis* account for the majority of candidiasis cases. Although the prevalence of *C. auris* among candidiasis patients is relatively low, concern is raising on its impact as a serious threat to public health due to three factors: (i) its diagnosis is difficult using standard methods, which may lead to non-optimal therapeutic choices; (ii) resistance against multiple antifungal drug families has been often identified in clinical isolates; and (iii) it causes outbreaks in healthcare settings (Satoh et al. 2009), possibly due to its ability to resist for long periods on hospital surfaces. The isolation of *C. auris* strains displaying resistance to the three main classes of available clinically used antifungal drugs (azoles, echinocandins, and polyenes), highlights the need to identify novel antifungal drug targets and design entirely new effective antifungal therapies.

Genome Scale Metabolic Models (GSMMs) are in silico reconstructions of global metabolic networks. They have been used to model the full metabolism of individual organisms (Zhang and Hua 2016), constituting a Systems Biology tool to analyse metabolic features (Gu et al. 2019). GSMMs have been used for decades for guiding strain design, in a metabolic engineering perspective. More recently, however, they have also been used in the elucidation of pathogenesis and drug target identification (Kim et al. 2010)[9]. Interestingly, such models have been built for the most clinically relevant *Candida* species, including *C. albicans* (Viana et al. 2020), *C. glabrata* (Xu et al. 2013) and *C. parapsilosis* (Viana et al. 2022), but not yet for *C. auris*. The exploitation of these GSMMs provide recent examples of the reliability of this approach in the identification of putative novel drug targets in pathogenic organisms.

Received 26 May 2023; **revised** 5 September 2023; **accepted** 17 October 2023
© The Author(s) 2023. Published by Oxford University Press on behalf of FEMS. All rights reserved. For permissions, please e-mail: journals.permissions@oup.com

Downloaded from https://academic.oup.com/femsyr/article/doi/10.1093/femsyr/foad045/7321573 by UMinho user on 12 September 2024

Herein, the construction and validation of the first GSMM for the human pathogen *C. auris* is described. This model is provided in the well-established SBML format and can easily be read in most metabolic engineering platforms, such as OptFlux (Rocha et al. 2010) and COBRA (Heirendt et al. 2019). A set of predicted essential genes was obtained from the validated model, and their targetability as putative novel antifungal drug targets is discussed. Additionally, the existent *Candida* GSMMs were exploited as a platform for cross-species comparison, aiming the analysis of their metabolic features, including the study of reactions and pathways which are common to all *Candida* species and the identification of reactions and pathways that are unique to each pathogen.

Materials and methods

Model construction

The metabolic model described here refers to the yeast *Candida auris* with the taxonomic ID 498019. Network reconstruction was performed using merlin 4.05 (Dias et al. 2015) and subsequent curation and validation were performed on OptFlux 3.0 (Rocha et al. 2010) using the IBM CPLEX 12.10 solver. Curation consisted of the editing, addition or removal of reactions so to correct previous gaps in the network using KEGG pathways, MetaCyc Database, and literature data as reference.

Enzyme and reaction annotation

Draft model construction consisted of an initial enzyme and reaction annotation from the reference genome sequence of the reference strain *Candida auris* B11221_V1, retrieved from NCBI's Assembly Database, accession ID "Cand_auris_B11221_V1" along with the respective Taxonomic ID (Federhen 2012). Genome wide functional annotation was performed by merlin by homology alignment assessment with resource to Basic Local Alignment Search Tool (BLAST) (Altschul et al. 1990) against the remote databases UniProtKB/Swiss-Prot (Boutet et al. 2016). Hit selection was performed as described in Dias et al. 2018 (Dias et al. 2018) and phylogenetic proximity was implemented based on phylogenetic tree from literature (Muñoz et al. 2018). The Kyoto Encyclopedia of Genes and Genomes (KEGG) (Kanehisa and Goto 2000) database served as reference for protein-reaction associations and consequent draft network construction.

Correcting reaction reversibility, directionality, and balance

Reaction reversibility curation comprised an initial automatic curation step followed by extensive manual curation. Automatic curation was performed by merlin referencing remote databases such as eQuilibrator (Flamholz et al. 2012), as described by Dias et al. (Dias et al. 2018). Manual curation referenced other databases such as Meta- Cyc (Caspi et al. 2014) as well as existing literature. Unbalanced reactions were identified automatically and manually balanced with resort to information from databases such as MetaCyc, ChEBI (Degtyarenko et al. 2008), Brenda (Schomburg et al. 2002), and existing literature. All manually edited reactions can be found in Supplementary file S1.

Compartmentalisation

The model described herein comprises four compartments: extracellular, cytoplasm, mitochondrion, peroxisome and one intercompartment: the cytoplasmic membrane. The online protein localisation predictor tool WoLF PSORT (Horton et al. 2007) was used in model compartmentalisation and was implemented on the already connected non-compartmentalised model through direct import of the report, as merlin has an integrated import tool for WoLF PSORT. Transport reactions—which connect the network compartments—were generated from the genome sequence with resort to the public database TCDB (Saier et al. 2021) and using merlin's integrated tool TranSyT (Lagoa 2019). Transport reactions across internal and external membranes for currency metabolites, such as H_2O, CO_2, and NH_3, often carried by facilitated diffusion, were added to the model with no gene association.

Defining the biomass equation

The biomass equation comprises all the cell's major components along with their respective relative numerical contributions—DNA, RNA, carbohydrates, lipids, and proteins—and was used as the objective function in all performed simulations, including essentiality prediction. The reconstructed model also includes ATP requirements for both biomass production and cell maintenance—growth-associated maintenance (GAM) and non-growth-associated maintenance (NGAM), respectively. A GAM value of 25.65 mmol ATP/gDCW was considered for the biomass equation, calculated based on the ATP requirements for the biosynthesis of cell polymers, as shown in Mishra et al. (Mishra et al. 2016), then adjusted for the considered biomass macromolecule composition. Non-growth-associated ATP maintenance was implemented in this model as an autonomous equation, thus forcing a basal ATP consumption—flux bounds inferred from *Candida tropicalis* (Mishra et al. 2016). The Supplementary file S1 details the biomass equation's components and their relative content. The theoretical ratio used in the *Saccharomyces cerevisiae* iMM904metabolic model for the phosphorus to-oxygen ratio was applied. Three generic reactions contributing to this ratio were automatically generated by merlin and were updated to replicate the same ratio as in the iRV973 model:

Reaction R00081:

$$1.0\ \mathrm{Oxygen_{mito}} + 4.0\ \mathrm{Ferrocytochrome\ c_{mito}} + 6.0\ \mathrm{H^{+}_{mito}} \leftrightarrow 2.0\ \mathrm{H_2O_{mito}} + 4.0\ \mathrm{Ferricytochrome\ c_{mito}} + 6.0\ \mathrm{H^{+}_{cyto}} \quad (1)$$

Reaction T02161:

$$1.0\ \mathrm{Ubiquinol_{mito}} + 2.0\ \mathrm{Ferricytochrome\ c_{mito}} + 1.5\ \mathrm{H^{+}_{mito}} \leftrightarrow 1.0\ \mathrm{Ubiquinone_{mito}} + 2.0\ \mathrm{Ferrocytochrome\ c_{mito}} + 1.5\ \mathrm{H^{+}_{cyto}} \quad (2)$$

Reaction T00485:

$$1.0\ \mathrm{Orthophosphate_{mito}} + 1.0\ \mathrm{ADPmito} + 3.0\ \mathrm{H^{+}_{cyto}} \leftrightarrow 1.0\ \mathrm{ATP_{mito}} + 1.0\ \mathrm{H_2O_{mito}} + 3.0\mathrm{H^{+}_{mito}} \quad (3)$$

The final balance reaction:

$$3.0\ \mathrm{Orthophosphate_{mito}} + 1.0\ \mathrm{Oxygen_{mito}} + 3.0\ \mathrm{ADP_{mito}} + 2.0\ \mathrm{Ubiquinol_{mito}} \leftrightarrow 3.0\ \mathrm{ATP_{mito}} + 5.0\ \mathrm{H_2O_{mito}} + 2.0\ \mathrm{Ubiquinone_{mito}} \quad (4)$$

Model simulations and enzyme essentiality prediction

Flux balance analysis (FBA) (Varma and Palsson 1994) on OptFlux 3.0 (Rocha et al. 2010) using the IBM CPLEX solver was used to conduct model simulations. Genes and reactions were considered

Downloaded from https://academic.oup.com/femsyr/article/doi/10.1093/femsyr/foad045/7321573 by UMinho user on 12 September 2024

essential if when removed from the model the resulting simulation's predicted biomass flux is less than 5% of the wild-type strain. Gene and reaction removal was simulated by restraining its corresponding flux bounds to zero. Gene/reaction essentiality was searched for in environmental conditions mimicking the human serum, namely the composition of the RPMI medium.

Model validation

Strains and growth media

Candida auris type strain B11221 was routinely maintained in Yeast extract–Peptone–Dextrose (YPD) and synthetic minimal media (SMM) was used for batch cultured experiments. YPD contained: 20 g/L glucose (Merck, Darmstadt, Germany), 20 g/L peptone (Merck, Darmstadt, Germany), and 10 g/L yeast extract (Merck, Darmstadt, Germany), while SMM included: 20 g/L glucose (Merck, Darmstadt, Germany), 2.7 g/L ammonium sulphate (Merck, Darmstadt, Germany), 0.05 g/L magnesium sulphate (Riddle-de-Haen), 2 g/L potassium dihydrogen phosphate (Panreac, Barcelona, Spain), 0.5 g/L calcium chloride (Merck, Darmstadt, Germany), and 100 μg/L biotin (Sigma).

Aerobic batch cultivation

Aiming the validation of the constructed model, *C. auris* B11221_V1 cells were batch cultivated in Erlenmeyer flasks containing 250 ml of SMM medium, at 30ºC (250 rpm). Exponential phase inocula (Optical Density at 600 nm (OD600nm) of 0.3) were prepared and cells were transferred to Erlenmeyer flasks containing 250 ml of fresh SMM medium and cultivated at 30ºC with orbital agitation (250 rpm) for 10 h.

Cell density, dry weight, and metabolite concentration assessment

Throughout cell cultivation in SMM 4 mL samples were retrieved every two hours for subsequent biomass and extracellular metabolite quantification, and cell density was monitored through OD_{600nm} measuring. For dry weight determination, culture samples were centrifuged at 13,000 rpm for 3 min and the pellets were lyophilised for 72 h at −80ºC and weighted. For extracellular metabolite identification and quantification and the concentrations of glucose, ethanol, glycerol, and acetic acid in the supernatants were determined by HPLC on an Aminex HPX-87 H Ion Exchange chromatography column, eluted with 0.0005 M H_2SO_4 at a flow rate of 0.6 mL/min at room temperature. Samples were analysed in triplicate and concentrations determined via adequate calibration curves. The specific growth rate, specific glucose consumption rate, and the specific production rates of ethanol, glycerol and acetic acid were calculated during the exponential growth phase as indicated elsewhere (Sauer et al. 1999).

Carbon and nitrogen source utilization assessment

The capability of utilizing different carbon and nitrogen sources for cell growth was assessed by comparing in silico predictions to the literature data for *C. auris*. For the carbon sources for which the model predictions were not consistent with literature data, experimental testing was conducted with the B11221 *C. auris* reference strain used in the model reconstruction, and also with representative strains from clades I and II, *C. auris* B8441 and *C. auris* B11220, respectively. The utilization of ethanol, glycerol, and galactitol as sole carbon source, by the *C. auris* strains was evaluated in solid YNB medium containing: either 5 g/L glucose as control, or 5 g/L of either one of the mentioned carbon sources; 1.7 g/L Yeast nitrogen base without amino-acids without ammonium sulfate (Sigma); 5 g/L Ammonium sulfate (Merck, Darmstadt, Germany) and 20 g/L Agar (Iberagar, Barreiro, Portugal). *C. auris* cell suspensions used to inoculate the agar plates, were mid-exponential cells grown in YNB medium with 5 g/L glucose, until culture OD600nm = 0.5 ± 0.05 was reached and then diluted in sterile water to obtain suspensions with OD600nm = 0.05 ± 0.005. These cell suspensions and subsequent dilutions (10^{-1}; 10^{-2}; 10^{-3}) were applied as 4 μL spots onto the surface of solid YNB media, with the indicated carbon sources. Growth was assessed after incubation at 37ºC for 48 hours.

Results and discussion

Model characteristics

The *C. auris* metabolic model, iRV973, comprises 973 genes associated with 2863 reactions—of which 352 are drains (exchange constraints for external metabolites used to simulate the environmental conditions and allow metabolites to be removed from the system) and 1035 are transport reactions—and 2150 metabolites across four compartments (extracellular, cytoplasm, mitochondria, and peroxisome) and within an intercompartment, the plasma membrane. The model can be found in SBML format in Supplementary file S2.

Manual curation assessed a total of 776 reactions requiring alterations, from which 75 were mass balanced and 701 were corrected regarding reversibility, directionality, annotation or added or removed from the model as detailed in Supplementary File S1.

The Biomass equation (Table 1) encompasses the cell's major components along with their respective and relative contributions, DNA, RNA, lipids, carbohydrates, and cofactors. The equation's composition in Carbohydrate (Pfaller and Riley 1992), Lipid (Ghannoum and Abu-Elteen 1990, Mishra et al. 2016), Sterol (Mishra et al. 2016), Phospholipid (Mishra et al. 2016), Fatty acid (Mayatepek et al. 2009) and Protein (Mishra et al. 2016) was inferred from literature data. On the other hand, for the composition of DNA, the whole genome sequence was used to estimate the amount of each deoxyribonucleotide as described in (Thiele and Palsson 2010), using the e-BiomassX merlin tool, while mRNA, rRNA, and tRNA were used to estimate the total RNA in the cell as described in (Thiele and Palsson 2010, Dias et al. 2014)), using the e-BiomassX merlin tool. The growth and non-growth ATP requirements were inferred from *C. tropicalis* (Mishra et al. 2016).

Model validation

Carbon and nitrogen source utilization

Simulations were performed in in silico SMM medium with different molecules as sole carbon and nitrogen sources and compared to phenotypic growth data from existing literature to assess iRV973's reliability in predicting biomass production from different sole carbon or nitrogen sources. Data related to *C. auris* strains, other than the reference B11221 strain, were also considered in the analysis to increase the number of carbon and nitrogen sources accounted for. A total of 36 sole carbon sources and 8 sole nitrogen sources were evaluated. In an initial assessment our model correctly predicted growth in 92% (33/36) of the carbon sources tested and in 100% (8/8) of the nitrogen sources. The model failed to predict growth in galactitol and wrongly predicted growth in ethanol and glycerol. However, since the literature data is based on strains different from the one used to reconstruct our model, CBS10913 (Satoh et al. 2009) and several other clinical isolates (Lee et al. 2011, Tamanna et al. 2022), we decided to test experimentally these 3 cases with one representative strain

Downloaded from https://academic.oup.com/femsyr/article/doi/10.1093/femsyr/foad045/7321573 by UMinho user on 12 September 2024

Table 1. Biomass composition used in the model iRV973. The full individual validated contributions of each of these metabolites are shown in Supplementary file S1.

Metabolite	g/gDCW	Metabolite	g/gDCW
Lipids[1]		**Proteins**[2]	
Lanosterol	0,000 054	L-Valine	0,021 208
Zymosterol	0,000 189	L-Tyrosine	0,025 060
5,7,22,24(28)-Ergostatetraenol	0,000 269	L-Tryptophan	0,015 297
Ergosterol	0,002 047	L-Threonine	0,011 456
Phosphatidylserine	0,018 028	L-Serine	0,004 758
Phosphatidylinositol	0,005 408	L-Proline	0,015 616
Phosphatidylcholine	0,008 089	L-Phenylalanine	0,021 862
Phosphatidylethanolamine	0,006 425	L-Methionine	0,007 562
Cardiolipin	0,003 883	L-Lysine	0,020 142
Tetradecanoic acid	0,000 026	L-Leucine	0,017 778
Hexadecanoic acid	0,001 329	L-Isoleucine	0,002 905
Octadecanoic acid	0,000 489	L-Histidine	0,016 385
Oleic acid	0,002 276	L-Glutamate	0,015 260
alpha-Linolenic acid	0,000 109	L-Cysteine	0,027 463
Triacylglycerol	0,013 575	L-Aspartate	0,014 186
Diacylglycerol	0,001 001	L-Asparagine	0,007 636
Sterol esters	0,014 687	L-Arginine	0,017 066
		L-Alanine	0,006 159
Carbohydrates[3]		Glycine	0,020 616
Chitin	0,026 552	L-Glutamine	0,009 458
Mannan	0,181 732		
β (1,3)-Glucan	0,381 756	**Soluble Pool**[4]	
		Thiamine	0,000 174
Ribonucleotides[5]		Ubiquinone-9	0,000 174
UTP	0,008 262	NADP+	0,000 174
GTP	0,006 585	NAD+	0,000 174
CTP	0,008 267	FMN	0,000 174
ATP	0,006 984	FAD	0,000 174
		CoA	0,000 174
Deoxyribonucleotides[5]		Biotin	0,000 174
dTTP	0,000 647	Pyridoxal phosphate	0,000 174
dGTP	0,000 537	5-Methyltetrahydrofolate	0,000 174
dCTP	0,000 534		
dATP	0,000 646		

[1](Ghannoum et al. 1990, Mago and Khuller 1990, Mayatepek et al. 2009)
[2](McVeigh and Bell 1951)
[3](Navarro-Arias et al. 2019)
[4](Xu et al. 2013)
[5]*Merlin e-BiomassX* Tool.

of *C. auris* clades I, II and III (B8441, B11220 and B11221). The results confirmed the model's prediction regarding the utilization of glycerol as carbon source and regarding the non-utilization of dulcitol (Fig. 1). Interestingly, none of the *C. auris* strains tested was able to grow in ethanol as the sole carbon source, contradicting the model's prediction and suggesting that, although having all the required enzymes for ethanol utilization, *C. auris* cannot use it, which may be due to regulatory reasons not accounted for in the model. Altogether our model only failed to predict growth in ethanol and was able to correctly predict 97% of the carbon sources tested (Table 2).

A particular case worth mentioning is the use of melezitose as a sole carbon source. According to the literature, it is known that *C. auris* is able to use this compound as a carbon source (Satoh et al. 2009, Lee et al. 2011, Cendejas-Bueno et al. 2012), this being a metabolic feature that distinguishes *C. auris* from other *Candida* species. However, as far as it could be assessed, there is no experimental evidence of any enzymes behind melezitose degradation. As far as we know, the pathway underlying melezitose degradation has never been identified in any system, making it impossible, considering the currently available knowledge, to add the corresponding reactions to the model.

Growth parameters in batch culture

Specific growth rate, glucose consumption rate and metabolite production rates were experimentally determined to validate the model quantitatively. A specific growth rate of 0.110 h^{-1} was observed for a glucose consumption rate of 2.19 mmol.gDCW^{-1}.h^{-1}, while no ethanol, glycerol or acetate production could be detected. In order to compare with the *in silico* results, a simulation of the system's behaviour in SMM medium, with a fixed glucose uptake flux of 2.19 mmol.g^{-1} dry weight.h^{-1} was performed to evaluate the model's ability to predict the specific growth rate. The remaining nutrient fluxes were left unconstrained, as the system in these conditions is glucose-limited. In this simulation the model predicted a specific growth rate of 0.155 h^{-1}, similar to the experimentally determined value (Table 3). Additionally, the formation of glycerol, acetic acid, and ethanol as by-products was not predicted to occur, which agrees with the experimental data and the notion that *C. auris* is a Crabtree-negative yeast.

Downloaded from https://academic.oup.com/femsyr/article/doi/10.1093/femsyr/foad045/7321573 by UMinho user on 12 September 2024

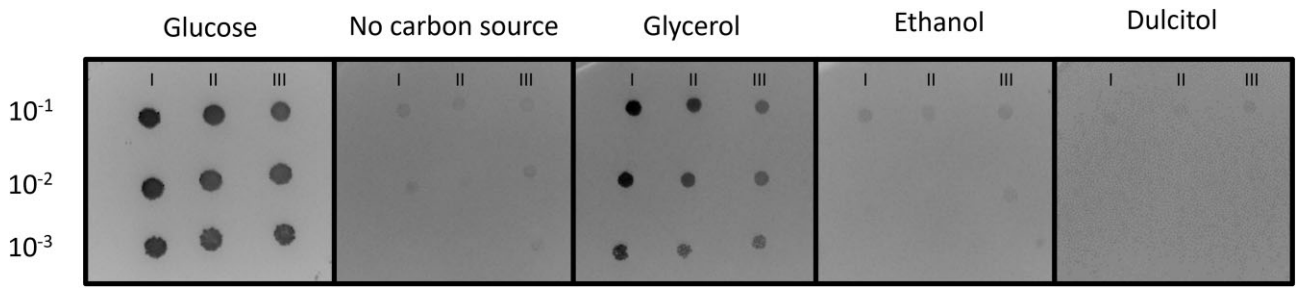


Figure 1. Utilization of glucose (positive control), no carbon source (negative control), glycerol, ethanol and dulcitol as carbon source by *C. auris* strains I: B8441 II: B11220 and III: B11221 in solid YNB medium. Initial OD600nm = 0.5 ± 0.05. Growth was assessed after incubation at 37°C for 48 h.

Table 2. Comparison between in vivo and in silico phenotypic behaviour of *C. auris* under different carbon and nitrogen sources.

	In vivo	*In silico*	Referece		*In vivo*	*In silico*	Referece
Carbon Source							
D-Glucose	+	+	1,4,5	D-Xylose	-	-	4
D-Glucosamine	-	-	4	L-Rhamnose	-	-	3,4
L-Arabinose	-	-	3,4	a,a-Trehalose	+	+	4,5
Sucrose	+	+	1,4,5	Salicin	-	-	4
β-D-galactoside	-	-	4	Raffinose	+	+	4
Melibiose	-	-	4	Starch	+	+	4
Glycerol	+	+	3,4	Ribitol	-	-	4
Xylitol	-	-	3,4	D-Mannitol	+	+	4
Galactitol	-	-	4	2-Keto-D-Gluconate	-	-	4
D-Gluconate	-	-	3,4	Succinate	-	-	3,4
Citrate	+	+	4	Ethanol	-	+	1,3,4
D-Galactose	-	-	3,4	Methanol	-	-	3,4
D-Ribose	-	-	4	N-acetylglucosamine	-	-	2,4
D-Arabinose	-	-	3,4				
Maltose	+	+	4,5	**Nitrogen Source**			
Cellobiose	-	-	4	Nitrite	-	-	4
Lactose	-	-	1,4	Cadaverine	+	+	4
Inulin	w	-	3,4	Nitrate	-	-	1,2,4
Erythritol	-	-	4	L-Lysine	+	+	4
D-Sorbitol	+	+	4	Ethylamine	-	-	4
myo-Inositol	-	-	4	Ammonia	+	+	4
DL-Lactate	-	-	4	Urea	-	-	2,4
L-Sorbose	-	-	3,4	Glycine	-	-	1

Growth (+); lack of growth (–); Weak Growth (W); 1:(Tamanna et al. 2022); 2:(Lee et al. 2011); 3:(Cendejas-Bueno et al. 2012); 4:(Satoh et al. 2009); 5:(Ninan et al. 2020).

Table 3. Growth parameters of iRV973 and comparison with experimentally determined values for *C. auris*.

	Specific growth rate (h-1)	q (mmol g-1 dry weight h-1)			
		Glucose consumption rate	Ethanol production rate	Glycerol production rate	Acetic acid production rate
In silico	0.153	2.19	0	0	0
In vivo	0.110	2.19	0	0	0

Candida auris unique metabolic features

To identify potentially unique metabolic features of *C. auris*, the iRV973 model was compared to the *C. glabrata* (Xu et al. 2013), *S. cerevisiae* (Mo et al. 2009), *C. albicans* (Viana et al. 2020) and *C. parapsilosis* (Viana et al. 2022) GSMMs. A comparison across the existing models was carried out based on shared EC number. After intersecting the EC numbers present in each of the five models, 88% (467/556) of the proteins with an associated EC number in the *C. auris* model were found to also be present in at least one of the other four models (Fig. 2). Additionally, although we found 37 EC numbers that appeared to be present in all *Candida* GSMMs and absent in the *S. cerevisiae* GSMM (Supplementary file S1), there are no enzymes present in all pathogenic yeasts and absent in *S. cerevisiae*. Although the initial inspection of the Candida GSMMs, when compared to the *S. cerevisiae* GSMM, suggested as much, upon further inspection, all the apparently "unique EC numbers" are just the result of changes in annotation and EC classification.

We found, additionally, 69 EC numbers to be exclusive to this model and may represent unique metabolic features of *C. auris*. However, among the 69 *C. auris* unique EC numbers, 41 are related to outdated/incomplete EC numbers or associated with other en-

Downloaded from https://academic.oup.com/femsyr/article/doi/10.1093/femsyr/foad045/7321573 by UMinho user on 12 September 2024

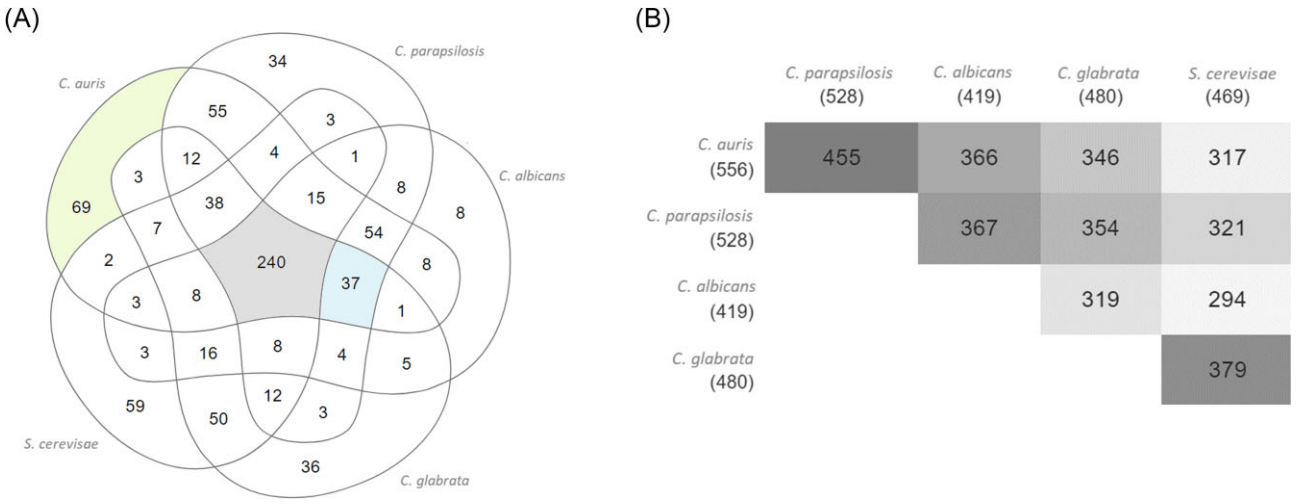


Figure 2. Comparison between *C. auris*, *C. parapsilosis*, *C. albicans*, *S. cerevisiae*, and *C. glabrata* proteins with associated EC Numbers present in the iRV973, iDC1003, iRV781, iIN800 and iNX804 genome-scale metabolic models, respectively. A: Venn Diagram. B: Pairwise Intersections. Diagrams were obtained using Multiple List Comparator (www.molbiotools.com).

zymes responsible for the same reactions in the different models. However, the following EC numbers (28) do stand out as potentially unique features of *C. auris*:

- 1.1.1.24: this EC number represents a quinate dehydrogenase that catalyses the oxidation of quinate to 3-dehydroquinate and is involved in quinate degradation, this enzyme seems to be a unique feature of *C. auris* among *Candida* species and may allow this yeast to utilize quinate as precursor for the biosynthesis of folates, quinones, and aromatic amino acids (Kubota et al. 2013).
- 1.1.1.10: this EC number represents a chloride peroxidase, which is able to catalyse the production of hypochlorous acid by transferring one oxygen atom from H_2O_2 to chloride. This is a very interesting feature since hypochlorous acid is used for microbial killing by phagocytic cells and in nature this enzyme is often associated with the production of halogenated antibiotics (van Schijndel et al. 1993). In *C. auris* this enzyme may represent a competitive advantage or even a potential mechanism of defence to the host.
- 1.13.11.24: this EC number represents a quercetinase which catalyses the degradation of quercetin, a molecule that exhibits antioxidant and antibacterial properties and is present in edible fruits and vegetables, being part of the human diet and also of soil composition due to degradation of those fruits. Some microorganisms exposed to these compounds developed the ability to degrade it (Merkens et al. 2008). This may be the case for *C. auris*.
- 3.1.1.65: this EC number represents a L-rhamnono-1,4-lactonase, which participates in the L-rhamnose degradation pathway. Although having some enzymes of this pathway, *C. auris* seems to be unable to use L-rhamnose as sole carbon source.

Drug target forecast based on gene essentiality prediction: a cross-species evaluation

IRV973 was used to identify potential new drug targets by determining enzyme essentiality. A list of essential reactions was obtained through simulation of the system's behaviour in RPMI medium, which mimics the environmental conditions of human serum, in order to narrow down the results to enzymes that should be essential in the conditions that a pathogen faces inside the host. A total of 158 reactions and 82 genes were predicted as essential in iRV973. The complete list of predicted essential genes and reaction in *C. auris* can be found in Supplementary file S1.

As seen before using a similar approach for *C. albicans* and *C. parapsilosis*, proteins which are targeted by currently used antifungal drugs were identified, including the targets of azoles, Erg11, and echinocandins, Fks1. This observation confirms the potential of using this approach in the quest for new drug targets. The most interesting outcome of this analysis, however, is the identification of numerous potential targets that are not currently used in clinical practice.

In the search for potential new antifungal drug targets suitable to be used against all forms of candidiasis, the enzymes predicted to be essential in *C. auris* were compared with those predicted to be essential in *C. albicans*, *C. parapsilosis* and *C. glabrata* (Xu et al. 2013, Viana et al. 2020, 2022). A total of 50 enzymes were predicted to be essential in the 4 species, according to the simulations run in the 4 corresponding GSMMs (Table 4). From this list we excluded drains, transport reactions and those without an associated or incomplete EC number. The 50 essential predicted enzymes can be grouped in 13 different pathways: steroid biosynthesis, purine metabolism, pyrimidine metabolism, terpenoid backbone biosynthesis, 1,3-beta-glucan biosynthesis, CoA biosynthesis, riboflavin metabolism, glycerophospholipid metabolism, ubiquinone biosynthesis, folate biosynthesis, oxidative phosphorylation, fatty acid biosynthesis and chitin biosynthesis. Some of these pathways are already targets of drugs used in clinical practice (Table 4), however, some could be explored as potential targets. In this work we not only propose these pathways as potential targets but also identify possible enzymes that should receive special focus in each of them.

For example, Erg4 (ergosterol biosynthesis), Chs2 (chitin biosynthesis) and Fol1 (folate biosynthesis) are targets without an orthologous enzyme in humans that are currently not targeted by any drug in *Candida* species. The absence of a human orthologous is a preferable attribute as this translates into lower

Downloaded from https://academic.oup.com/femsyr/article/doi/10.1093/femsyr/foad045/7321573 by UMinho user on 12 September 2024

Table 4. Enzymes predicted to be essential in RPMI medium, based on the screening of the genome-scale metabolic models of *C. auris* IRV973, *C. parapsilosis* iDC1003, *C. albicans* iRV781, and *C. glabrata* iNX804. Bold: fungal-specific enzymes. Data regarding the drug association retrieved from DrugBank database; only drugs with known pharmacological action against pathogens were selected.

Gene name						Pharmacological action	EC Number	Pathway
C. auris	*C. albicans*	*C. glabrata*	*C. parapsilosis*	*S. cerevisiae*	Human			
CJI97_000 938	*ERG26*	*CAGL0G00594g*	*CPAR2_302 110*	*ERG26*	*NSDHL*	-	1.1.1.170	Steroid biosynthesis
CJI97_000 080	*IMH3*	*CAGL0K10780g*	*CPAR2_104 580*	*IMD4*	*IMPDH*	-	1.1.1.205	Purine metabolism
CJI97_004 310	*ERG27*	*CAGL0M11506g*	*CPAR2_801 560*	*ERG27*	*DHRS11*	-	1.1.1.270	Steroid biosynthesis
CJI97_003 299	*HMG1*	*CAGL0L11506g*	*CPAR2_110 330*	*HMG1*	*HMGCR*	-	1.1.1.34	Terpenoid backbone biosynthesis
CJI97_003 097	*ERG24*	*CAGL0I02970g*	*CPAR2_405 900*	*ERG24*	*TM7SF2*	-	1.3.1.70	Steroid biosynthesis
CJI97_002 908	**ERG4**	**ERG4**	**ERG4**	**ERG4**	**-**	-	**1.3.1.71**	Steroid biosynthesis
CJI97_005 101	*CDC21*	*CDC21*	*CPAR2_206 550*	*TMP1*	*TYMS*	-	2.1.1.45	Pyrimidine metabolism
CJI97_002 511	*ADE17*	*CAGL0A03366g*	*CPAR2_202 250*	*ADE17*	*ATIC*	-	2.1.2.3	Purine metabolism
CJI97_002 269	*URA2*	*CAGL0L05676g*	*CPAR2_203 160*	*URA2*	*CAD*	-	2.1.3.2	Pyrimidine metabolism
FKS1	**GSC1**	**FKS1**	**CPAR2_106 400**	**FKS1**	**-**	**Echinocandins**	**2.4.1.34**	1,3-beta-glucan biosynthesis
CJI97_002 422	*URA5*	*URA5*	*CPAR2_802 790*	*URA5*	*UMPS*	-	2.4.2.10	Pyrimidine metabolism
CJI97_001 833	*ADE4*	*CAGL0M13717g*	*CPAR2_208 260*	*ADE4*	*PPAT*	-	2.4.2.14	Purine metabolism
CJI97_003 197	*BTS1*	*CAGL0H05269g*	*CPAR2_302 840*	*BTS1*	*GGPS1*	-	2.5.1.1	Terpenoid backbone biosynthesis
CJI97_001 757	*ERG20*	*ERG20*	*CPAR2_103 950*	*ERG20*	*FDPS*	-	2.5.1.10	Terpenoid backbone biosynthesis
CJI97_003 836	*C5_05130C*	*CAGL0F05555g*	*CPAR2_502 760*	*CAB5*	*COASY*	-	2.7.1.24	CoA biosynthesis
CJI97_005 311	*CR_03740C*	*CAGL0K11022g*	*CPAR2_202 590*	*FMN1*	*RFK*	-	2.7.1.26	Riboflavin metabolism
CJI97_004 586	*C6_02980C*	*CAGL0H01551g*	*CPAR2_602 050*	*CAB1*	*PANK*	-	2.7.1.33	CoA biosynthesis
CJI97_000 033	*URA6*	*CAGL0L09867g*	*CPAR2_105 320*	*URA6*	*CMPK2*	-	2.7.4.14	Pyrimidine metabolism
CJI97_001 215	*ERG8*	*ERG8*	*CPAR2_400 710*	*ERG8*	*PMVK*	-	2.7.4.2	Terpenoid backbone biosynthesis
CJI97_000 019	*C5_00260W*	*CAGL0D00550g*	*CPAR2_304 260*	*PRS1*	*PRPS1*	-	2.7.6.1	Purine metabolism
CJI97_005 306	*C4_05210W*	*CAGL0G03157g*	*CPAR2_500 260*	*PIS1*	*CDIPT*	-	2.7.8.11	Glycerophospholipid metabolism
CJI97_002 826	*ADE8*	*CAGL0F02761g*	*CPAR2_211 620*	*ADE8*	*GART*	-	2.1.2.2	Purine metabolism
CJI97_005 452	*COQ3*	*CAGL0I07601g*	*CPAR2_602 300*	*COQ3*	*COQ3*	-	2.1.1.114	Ubiquinone biosynthesis
CJI97_003 704	*COQ5*	*CAGL0J06710g*	*CPAR2_209 250*	*COQ5*	*COQ5*	-	2.1.1.201	Ubiquinone biosynthesis
ERG11	*ERG11*	*ERG11*	*ERG11*	*ERG11*	*CYP51A1*	Azoles	1.14.14.154	Steroid biosynthesis
CJI97_000 224	*PEL1*	*PGS1*	*CPAR2_805 350*	*PEL1*	*PGS1*	-	2.7.8.5	Glycerophospholipid metabolism
CJI97_004 676	*C1_08780W*	*PHO8*	*CPAR2_804 250*	*PHO8*	*ALPL*	-	3.1.3.1	Folate biosynthesis
CJI97_005 490	*C6_01340C*	*CAGL0H04389g*	*CPAR2_602 700*	*GEP4*	*PTPMT1*	-	3.1.3.27	Glycerophospholipid metabolism

Downloaded from https://academic.oup.com/femsyr/article/doi/10.1093/femsyr/foad045/7321573 by UMinho user on 12 September 2024

Table 4. Continued

Gene name						Pharmacological action	EC Number	Pathway
C. auris	*C. albicans*	*C. glabrata*	*C. parapsilosis*	*S. cerevisiae*	Human			
CJI97_002 941	*URA4*	*CAGL0J04598g*	*CPAR2_100 500*	*URA4*	*CAD*	-	3.5.2.3	Pyrimidine metabolism
CJI97_000 499	*IPP1*	*IPP1*	*CPAR2_806 200*	*IPP1*	*PPA2*	-	3.6.1.1	Oxidative phosphorylation
CJI97_004 071	*ADE2*	*ADE2*	*CPAR2_805 940*	*ADE2*	*PAICS*	-	4.1.1.21	Purine metabolism
CJI97_003 384	*URA3*	*URA3*	*URA3*	*URA3*	*UMPS*	-	4.1.1.23	Pyrimidine metabolism
CJI97_001 340	*MVD*	*CAGL0C03630g*	*CPAR2_109 530*	*MVD1*	*MVD*	-	4.1.1.33	Terpenoid backbone biosynthesis
CJI97_003 563	*CAB3*	*CAGL0L05302g*	*CPAR2_800 750*	*CAB3*	*PPCDC*	-	4.1.1.36	CoA biosynthesis
CJI971_001 274	**FOL1**	**CAGL0J07920g**	**CPAR2_303 390**	**FOL1**	**-**	**Sulfacetamide**	**4.1.2.25**	Folate biosynthesis
CJI971_001 274	**FOL1**	**CAGL0J07920g**	**CPAR2_303 390**	**FOL1**	**-**	**Sulfonamides**	**2.5.1.15**	Folate biosynthesis
CJI97_000 801	*ADE13*	*CAGL0B02794g*	*CPAR2_204 960*	*ADE13*	*ADSL*	-	4.3.2.2	Purine metabolism
CJI97_001 183	*IDI1*	*CAGL0J06952g*	*CPAR2_401 630*	*IDI1*	*IDI1*	-	5.3.3.2	Terpenoid backbone biosynthesis
CJI97_005 090	*ERG7*	*CAGL0J10824g*	*CPAR2_301 800*	*ERG7*	*LSS*	Oxiconazole	5.4.99.7	Steroid biosynthesis
CJI97_003 065	*ADE1*	*CAGL0I04444g*	*CPAR2_500 190*	*ADE1*	*PAICS*	-	6.3.2.6	Purine metabolism
CJI97_001 704	*ADE5,7*	*CAGL0H07887g*	*CPAR2_208 400*	*ADE5,7*	*GART*	-	6.3.3.1	Purine metabolism
CJI97_001 704	*ADE5,7*	*CAGL0H07887g*	*CPAR2_208 400*	*ADE5,7*	*GART*	-	6.3.4.13	Purine metabolism
CJI97_002 160	*ADE6*	*CAGL0K04499g*	*CPAR2_204 070*	*ADE6*	*PFAS*	-	6.3.5.3	Purine metabolism
CJI97_001 038	*ACC1*	*CAGL0L10780g*	*CPAR2_804 060*	*ACC1*	*ACACA*	-	6.4.1.2	Fatty acid biosynthesis
CJI97_005 606	*ERG12*	*CAGL0F03861g*	*CPAR2_803 530*	*ERG12*	*MVK*	-	2.7.1.36	Terpenoid backbone biosynthesis
CJI97_004 952	*ERG13*	*ERG13*	*CPAR2_701 400*	*ERG13*	*HMGCS*	-	2.3.3.10	Terpenoid backbone biosynthesis
CJI97_001 309	**FAS1**	**CAGL0D00528g**	**FAS1**	**FAS1**	**-**	-	**2.3.1.86**	Fatty acid biosynthesis
CJI97_005 609	*GUA1*	*CAGL0F03927g*	*CPAR2_803 560*	*GUA1*	*GMPS*	-	6.3.5.2	Pyrimidine metabolism
CJI97_004 456	*URA7*	*URA7*	*CPAR2_100 620*	*URA7*	*CTPS1*	-	6.3.4.2	Pyrimidine metabolism
CHS2	**CHS1**	**CAGL0I04818g**	**CPAR2_805 640**	**CHS2**	**-**	-	**2.4.1.16**	Chitin biosynthesis

Downloaded from https://academic.oup.com/femsyr/article/doi/10.1093/femsyr/foad045/7321573 by UMinho user on 12 September 2024

chances of host drug toxicity and may allow for greater freedom of drug design, making these targets good candidates for drug targeting. However, the potential of the remaining candidates should not be discarded. Indeed, there are several reported cases of drug targets for which there are human orthologs. In those cases, the drug specificity relies on its design favouring affinity to the pathogen's target, when compared to the eventual human target.

Conclusions

This study presents the first validated global metabolic model for the human pathogen *C. auris*. The manual curation and experimental validation of the model have demonstrated its capability to quantitatively predict the main metabolic features of *C. auris* and its utilization of various metabolites as sole carbon or nitrogen sources. The overlap of 88% of the proteins with associated EC numbers in other already published yeast models establishes a foundation of shared metabolic pathways among yeast species. Notably, 28 exclusive proteins in this model may unveil unique metabolic characteristics specific to *C. auris*.

The utilization of iRV973 to predict essential genes in RPMI medium has unveiled a list of potential drug targets. Remarkably, 50 of these essential genes have been predicted as vital in all *Candida* species for which GSMMs are available. Among these identified potential drug targets, some encode proteins already known to be targets of antifungal agents and other antimicrobial agents used in clinical practice, demonstrating the potential of this approach in identifying new drug targets. Of particular interest are the enzymes lacking any human homolog or drug association, making them highly promising candidates as new drug targets. Targeting such enzymes could lead to novel therapeutic strategies with reduced risks of off-target effects on human cells.

Looking to the future, this validated global metabolic model for *C. auris* opens exciting prospects for further research and applications. It can be used as a platform to investigate the metabolic network of *C. auris* and with advancements in computational biology and systems biology, this model could be further refined and expanded to encompass additional aspects of the pathogen's biology, as well as offering potential new clues for therapeutic approaches against *C. auris*.

Supplementary data

Supplementary data is available at *FEMSYR Journal* online.

Conflict of interest: None declared.

Funding

This work was supported by "Fundação para a Ciência e a Tecnologia" (FCT) (Contract PTDC/BII-BIO/28216/2017 and AEM PhD grant to RV). Funding received from project LISBOA-01-0145-FEDER-022231-the BioData.pt Research Infrastructure is acknowledged. This work was further financed by national funds from FCT in the scope of the project UIDB/04565/2020 and UIDP/04565/2020 of the Research Unit Institute for Bioengineering and Biosciences—iBB, project UIDB/04469/2020 for the Centre of Biological Engineering—CEB, and the project LA/P/0140/2020 of the Associate Laboratory Institute for Health and Bioeconomy—i4HB.

References

Ademe M, Girma F. Candida auris: from multidrug resistance to pan-resistant strains. *Infect Drug Resist* 2020;**13**:1287–94. https://doi.org/10.2147/IDR.S249864

Altschul SF, Gish W, Miller W *et al.* Basic local alignment search tool. *J Mol Biol* 1990;**215**:403–10. https://doi.org/10.1016/S0022-2836(05)80360-2

Boutet E, Lieberherr D, Tognolli M *et al.* UniProtKB/Swiss-Prot, the manually annotated section of the UniProt KnowledgeBase: how to use the entry view. *Methods Mol Biol* 2016;**1374**:23–54. https://doi.org/10.1007/978-1-4939-3167-5_2

Caspi R, Altman T, Billington R *et al.* The MetaCyc database of metabolic pathways and enzymes and the BioCyc collection of Pathway/Genome databases. *Nucleic Acids Res* 2014;**44**:D471–80. https://doi.org/10.1093/nar/gkt1103

Cendejas-Bueno E, Kolecka A, Alastruey-Izquierdo A *et al.* Reclassification of the *Candida haemulonii* complex as *Candida haemulonii* (*C. haemulonii* group I), *C. duobushaemulonii* sp. nov. (*C. haemulonii* group II), and *C. haemulonii var. Vulnera var. nov.*: three multiresistant human pathogenic yeasts. *J Clin Microbiol* 2012;**50**:3641–51. https://doi.org/10.1128/JCM.02248-12

Degtyarenko K, De matos P, Ennis M *et al.* ChEBI: a database and ontology for chemical entities of biological interest. *Nucleic Acids Res* 2008;**36**:D344–50. https://doi.org/10.1093/nar/gkm791

Dias O, Pereira R, Gombert AK *et al.* iOD907, the first genome-scale metabolic model for the milk yeast *Kluyveromyces lactis*. *Biotechnol J* 2014;**9**:776–90. https://doi.org/10.1002/biot.201300242

Dias O, Rocha M, Ferreira EC *et al.* Reconstructing genome-scale metabolic models with merlin. *Nucleic Acids Res* 2015;**43**:3899–910. https://doi.org/10.1093/nar/gkv294

Dias O, Rocha M, Ferreira EC *et al.* Reconstructing high-quality large-scale metabolic models with merlin. In: *Methods Mol Biol* 2018;**1716**:1–36. https://doi.org/10.1007/978-1-4939-7528-0_1

Federhen S. The NCBI Taxonomy database. *Nucleic Acids Res* 2012;**40**:D136–43. https://doi.org/10.1093/nar/gkr1178

Flamholz A, Noor E, Bar-Even A *et al.* EQuilibrator - the biochemical thermodynamics calculator. *Nucleic Acids Res* 2012;**40**:770–5. https://doi.org/10.1093/nar/gkr874

Ghannoum MA, Abu-Elteen KH. Pathogenicity determinants of *Candida*. *Mycoses* 1990;**33**:265–82. https://doi.org/10.1111/myc.1990.33.6.265

Ghannoum MA, Swairjo I, Soll DR. Variation in lipid and sterol contents in *Candida albicans* white and opaque phenotypes. *Med Mycol* 1990;**28**:103–15. https://doi.org/10.1080/02681219080000151

Gu C, Kim GB, Kim WJ *et al.* Current status and applications of genome-scale metabolic models. *Genome Biol* 2019;**20**:121. https://doi.org/10.1186/s13059-019-1730-3

Heirendt L, Arreckx S, Pfau T *et al.* Creation and analysis of biochemical constraint-based models using the COBRA Toolbox v.3.0. *Nat Protoc* 2019;**14**:639–702. https://doi.org/10.1038/s41596-018-0098-2

Horton P, Park KJ, Obayashi T *et al.* WoLF PSORT: protein localization predictor. *Nucleic Acids Res* 2007;**35**:W585–7. https://doi.org/10.1093/nar/gkm259

Kanehisa M, Goto S. KEGG: kyoto Encyclopedia of Genes and Genomes. *Nucleic Acid Research* 2000;**28**:27–30. https://doi.org/10.1093/nar/28.1.27

Kim MN, Shin JH, Sung H *et al. Candida haemulonii* and closely related species at 5 university hospitals in Korea: identification, antifungal susceptibility, and clinical features. *Clin Infect Dis* 2009;**48**:57–61. https://doi.org/10.1086/597108

Downloaded from https://academic.oup.com/femsyr/article/doi/10.1093/femsyr/foad045/7321573 by UMinho user on 12 September 2024

Kim TY, Kim HU, Lee SY. Metabolite-centric approaches for the discovery of antibacterials using genome-scale metabolic networks. *Metab Eng* 2010;**12**:105–11. https://doi.org/10.1016/j.ymben.2009.05.004

Kubota T, Tanaka Y, Hiraga K *et al.* Characterization of shikimate dehydrogenase homologues of *Corynebacterium glutamicum*. *Appl Microbiol Biotechnol* 2013;**97**:8139–49. https://doi.org/10.1007/S00253-012-4659-Y

Lagoa D. *Development of Bioinformatics Tools for the Classification of Transporter Systems*. University of Minho: Braga 2019.

Lass-Flörl C. The changing face of epidemiology of invasive fungal disease in Europe. *Mycoses* 2009;**52**:197–205. https://doi.org/10.1111/j.1439-0507.2009.01691.x

Lee WG, Shin JH, Uh Y *et al.* First three reported cases of nosocomial fungemia caused by *Candida auris*. *J Clin Microbiol* 2011;**49**:3139–42. https://doi.org/10.1128/JCM.00319-11

Mago N, Khuller GK. Lipids of *Candida albicans*: subcellular distribution and biosynthesis. *J Gen Microbiol* 1990;**136**:993–6. https://doi.org/10.1099/00221287-136-6-993

Mayatepek E, Herz A, Leichsenring M *et al.* Fatty acid analysis of different Candida, species by capillary column gas-liquid chromatography. *Mycoses* 2009;**34**:1–2. https://doi.org/10.1111/j.1439-0507.1991.tb00619.x

McVeigh I, Bell E. The amino acid and vitamin requirements of *Candida albicans* Y-475 and *mycoderma vini* Y-939. *Bulletin Torrey Botanical Club* 1951;**78**:134–44. https://doi.org/10.2307/2482046

Merkens H, Kappl R, Jakob RP *et al.* Quercetinase QueD of *Streptomyces* sp. FLA, a monocupin dioxygenase with a preference for nickel and cobalt. *Biochemistry* 2008;**47**:12185–96. https://doi.org/10.1021/bi801398x.

Mishra P, Park GY, Lakshmanan M *et al.* Genome-scale metabolic modeling and in silico analysis of lipid accumulating yeast *Candida tropicalis* for dicarboxylic acid production. *Biotechnol Bioeng* 2016;**113**:1993–2004. https://doi.org/10.1002/bit.25955

Mo ML, Palsson B, Herrgård MJ. Connecting extracellular metabolomic measurements to intracellular flux states in yeast. *BMC Syst Biol* 2009;**3**:37. https://doi.org/10.1186/1752-0509-3-37

Muñoz JF, Gade L, Chow NA *et al.* Genomic insights into multidrug-resistance, mating and virulence in *Candida auris* and related emerging species. *Nat Commun* 2018;**9**:5346. https://doi.org/10.1038/s41467-018-07779-6

Navarro-Arias MJ, Hernández-Chávez MJ, García-Carnero LC *et al.* Differential recognition of *Candida tropicalis*, *Candida guilliermondii*, *Candida krusei*, and *Candida auris* by human innate immune cells. *Infect Drug Resist* 2019;**12**:783–94. https://doi.org/10.2147/IDR.S197531

Ninan MM, Sahni RD, Chacko B *et al.* *Candida auris*: clinical profile, diagnostic challenge and susceptibility pattern: experience from a tertiary-care centre in South India. *J Global Antimicrob Resist* 2020;**21**:181–5. https://doi.org/10.1016/j.jgar.2019.10.018

Pfaller M, Riley J. Effects of fluconazole on the sterol and carbohydrate composition of four species of *Candida*. *Eur J Clin Microbiol Infect Dis* 1992;**11**:152–6. https://doi.org/10.1007/BF01967067

Rocha I, Maia P, Evangelista P *et al.* OptFlux: an open-source software platform for in silico metabolic engineering. *BMC Syst Biol* 2010;**4**:45. https://doi.org/10.1186/1752-0509-4-45

Saier MH, Reddy VS, Moreno-Hagelsieb G *et al.* The transporter classification database (TCDB): 2021 update. *Nucleic Acids Res* 2021;**49**:D461–7. https://doi.org/10.1093/nar/gkaa1004

Satoh K, Makimura K, Hasumi Y *et al.* *Candida auris* sp. nov., a novel ascomycetous yeast isolated from the external ear canal of an inpatient in a Japanese hospital. *Microbiol Immunol* 2009;**53**:41–4. https://doi.org/10.1111/j.1348-0421.2008.00083.x

Sauer U, Lasko DR, Fiaux J *et al.* Metabolic flux ratio analysis of genetic and environmental modulations of *Escherichia coli* central carbon metabolism. *J Bacteriol* 1999;**181**:6679–88. https://doi.org/10.1128/jb.181.21.6679-6688.1999

Schomburg I, Chang A, Schomburg D. BRENDA, enzyme data and metabolic information. *Nucleic Acids Res* 2002;**30**:47–49. https://doi.org/10.1093/nar/30.1.47

Tamanna P, Saifali A, Jayati C *et al.* Comprehensive characterization of *Candida* isolates in a given geographical area for the determination of prevalence and drug sensitivity. MedRxiv. 2022.

Thiele I, Palsson B. A protocol for generating a high-quality genome-scale metabolic reconstruction. *Nat Protoc* 2010;**5**:93–121. https://doi.org/10.1038/nprot.2009.203

van Schijndel JWPM, Vollenbroek EGM, Wever R. The chloroperoxidase from the fungus *curvularia inaequalis*; a novel vanadium enzyme. *Biochim Biophys Acta* 1993;**1161**:249–56. https://doi.org/10.1016/0167-4838(93)90221-C

Varma A, Palsson BO. Stoichiometric flux balance models quantitatively predict growth and metabolic by-product secretion in wild-type *Escherichia coli* W3110. *Appl Environ Microbiol* 1994;**60**:3724–31. https://doi.org/10.1128/aem.60.10.3724-3731.1994

Viana R, Couceiro D, Carreiro T *et al.* A genome-scale metabolic model for the Human pathogen *Candida Parapsilosis* and early identification of putative novel antifungal drug targets. *Genes* 2022;**13**:303. https://doi.org/10.3390/genes13020303

Viana R, Dias O, Lagoa D *et al.* Genome-scale metabolic model of the Human pathogen *Candida albicans*: a promising platform for drug target prediction. *J Fungi* 2020;**6**:171. https://doi.org/10.3390/jof6030171

Xu N, Liu L, Zou W *et al.* Reconstruction and analysis of the genome-scale metabolic network of *Candida glabrata*. *Mol Biosyst* 2013;**9**:205–16. https://doi.org/10.1039/c2mb25311a

Zhang C, Hua Q. Applications of genome-scale metabolic models in biotechnology and systems medicine. *Front Physiol* 2016;**6**:1–8. https://doi.org/10.3389/fphys.2015.00413

Downloaded from https://academic.oup.com/femsyr/article/doi/10.1093/femsyr/foad045/7321573 by UMinho user on 12 September 2024

Received 26 May 2023; **revised** 5 September 2023; **accepted** 17 October 2023
© The Author(s) 2023. Published by Oxford University Press on behalf of FEMS. All rights reserved. For permissions, please e-mail: journals.permissions@oup.com